

Probing *trans*-polyacetylene segments in a diamond film by tip-enhanced Raman spectroscopy

Leyong Hu^{a,b}, Yang Guo^{a,b,*}, Shuo Du^{a,b}, Shibing Tian^{a,b}, Junjie Li^{a,b,c}, Changzhi Gu^{a,b,*}

^a Beijing National Laboratory for Condensed Matter Physics, Institute of Physics, Chinese Academy of Sciences, Beijing 100190, People's Republic of China

^b School of Physical Sciences, CAS Key Laboratory of Vacuum Physics, University of Chinese Academy of Sciences, Beijing 100190, People's Republic of China

^c Songshan Lake Materials Laboratory, Dongguan 523808, People's Republic of China

ARTICLE INFO

Keywords:

TERS
Nanodiamond
Trans-polyacetylene

ABSTRACT

As an important carbon material, a nano-crystalline diamond (NCD) film is very promising in the field of science and technology. However, there are little knowledge about surface physics and chemistry of nanoscale in NCD films. Here, we perform nanoscale imaging of NCD films grown by hot filament chemical vapor deposition, using tip-enhanced Raman spectroscopy. With ~ 20 nm spatial resolution, we resolve nanoscale spatial correlations of *trans*-polyacetylene segments on the surface with characterized Raman modes at 1150 cm^{-1} and 1480 cm^{-1} that originate from the motion of conjugate polymer skeletons with a substantial contribution from the in-plane bending of carbon-hydrogen bonds and stretching vibrations of the double carbon-carbon bonds. Our work is helpful to understand the role of TPA in NCD synthesis reaction in nanoscale and improve the device application based on this material.

1. Introduction

The development of carbon material science has been throughout human history. A typical example is a diamond film, which is always fascinating due to its unique combination of outstanding properties (including the highest hardness, high thermal conductivity, large band gap, excellent chemical stability and biocompatibility) [1–4]. Since beginning in the late 1990s the synthesis of polycrystalline diamond films with small grains known as nano-crystalline diamond (NCD) has made great achievements, which leads to the utilization of outstanding diamond properties and development of a wide range of applications in various fields of engineering [5–7], such as Micro Electro Mechanical System (MEMS) devices, optical coatings, lateral field emission diodes, biosensors, surface acoustic wave (SAW) filters, etc. [8,9].

Conventional polycrystalline semiconductors such as silicon are composed of a large number of grains and grain boundaries. And grain boundaries contain those atoms that have been perturbed from their original lattice sites, dislocations, and impurities. However, the atom structure of grain boundaries in NCD is greatly different from them and more complicated, because the part of excess energy of the grain boundaries is relaxed by changing the hybridization of carbon atoms to form more ordered sp^2 -bonded carbon structures, which allow for

existence of various nanostructures and chemical phases [8,10,11]. Moreover, other inclusions such as amorphous graphite and $C-H_x$ chains could be formed on the surface of a NCD film because of the non-equilibrium growth conditions, even though it has a smooth surface. For example, observations by transmission electron microscopy have showed that nano-diamond particles are polyhedra consisting of a diamond core built up of sp^3 carbon, which may be partially coated by a graphitic shell or amorphous carbon with dangling bonds terminated by functional groups [8,12]. Raman measurements have demonstrated that *trans*-polyacetylene (TPA) segments become formed at grain boundaries and the surface of NCD films, as evidenced by the characteristic Raman bands of ν_3 (C-H in plane bending) at 1150 cm^{-1} and ν_1 (C=C stretch) at 1480 cm^{-1} [13–16]. In fact, few attentions were paid on the effect of TPA segments on the synthesis reaction or the physical properties of NCD films in the previous studies, although it was recognized as the first conducting polymer in 1976, leading to the development of the field of organic conducting polymers [17,18].

Therefore, more work is needed to study the surface physics and chemistry of diamond films in nanoscale, which is going to provide a deeper understanding of the diamond growth of non-equilibrium thermodynamics. In this regard, tip-enhanced Raman spectroscopy (TERS) Raman spectroscopy has proven to be a powerful tool to accomplish this

* Corresponding authors at: Beijing National Laboratory for Condensed Matter Physics, Institute of Physics, Chinese Academy of Sciences, Beijing 100190, People's Republic of China.

E-mail addresses: yangguo@iphy.ac.cn (Y. Guo), czgu@iphy.ac.cn (C. Gu).

<https://doi.org/10.1016/j.diamond.2021.108415>

Received 17 February 2021; Received in revised form 7 April 2021; Accepted 16 April 2021

Available online 24 April 2021

0925-9635/© 2021 Elsevier B.V. All rights reserved.

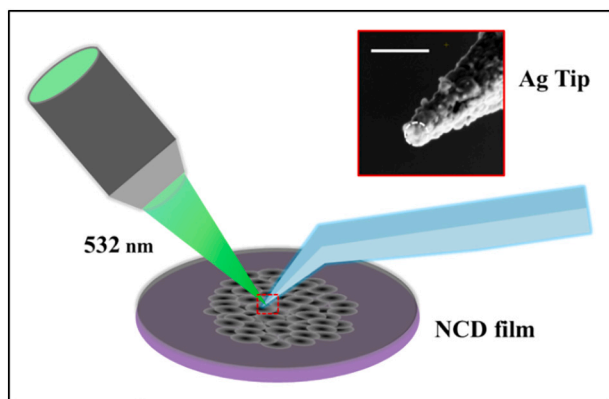


Fig. 1. Schematic for tip enhanced Raman scattering from NCD films. The excitation light at 532 nm was focused on the tip through an objective (Mitutoyo, M Plan Apo 100 \times , NA = 0.7) mounted at 45 degree. The TERS tip is a silver-covered silicon cone with a radius of curvature about 100 nm. The inset is a SEM image of the TERS tip with a scale bar of 500 nm.

goal, which brings Raman spectroscopy into nanoscale resolution imaging [19–21]. TERS is a super-resolution chemical technique, which is performed in an integrated system combined of Raman spectrometer and Scanning Probe microscope (SPM), for example atomic force microscope (AFM) or scanning tunneling microscope. A TERS system is based on a metallic tip employed to concentrate the incident light field at the apex, greatly improving the Raman sensitivity and reducing the probed volume to the nanoscale region immediately below the tip [22]. While TERS has already been used to study various carbon materials such as graphene [23,24], carbon tubes [25,26], amorphous carbon films and carbon anions [27]. In particular, this technology shows great advantages in practical application research such as commercial hard disk drives, tribology and lubricant detection et al. [28,29] But to our best

knowledge, it is rarely used to nanoscale image chemical components in diamond films. Here, we perform resonant TERS imaging of NCD films. We demonstrate the advantage of TERS for nanoscale imaging of the surface of NCD films and identification of locally spatial distribution of TPA segments on surface.

2. Experimental section

2.1. Synthesis of diamond films

In our study, the diamond films were grown on 4-in. n-doped Si (100) wafers by the hot filament chemical vapor deposition (HFCVD) [30]. Before the deposition process, the substrate was pretreated with a diamond-enhanced nucleation solution which is 20% diamond nanoparticles-stock solution in methanol, so that the diamond particles were immersed into the substrate surface by ultrasound. The pretreatment step was followed by cleaning the substrate with methanol, isopropanol and acetone in sequence. And then, the substrate was placed in a HFCVD vacuum chamber. During growth, the temperature of a Ta filament was 2200 $^{\circ}$ C and it was kept at a distance of 15 mm from the substrate with 750 $^{\circ}$ C. The flow ratio of hydrogen (H_2) and methane (CH_4) was 150:10.5 sccm under a low working pressure of 3 KPa, which resulted in a growth rate of \sim 625 nm/h. The average thickness of the diamond film is about 5 μ m.

2.2. Characterization

The high-power transfer target polycrystalline X-ray diffractometer (Mac Science M18XHF) was used to analyze the crystal structure of the sample with $Cu_{K\alpha}$ as the X-ray source. The continuous scanning was performed using a $2\theta/\theta$ coupled scanning method with a step width of 0.02° and the tube voltage is 40 KV. The morphology and cross section of the diamond film was observed by scanning electron microscope (FEI Helios 600I). Raman spectroscopy (Horiba HR Evolution) and X-ray

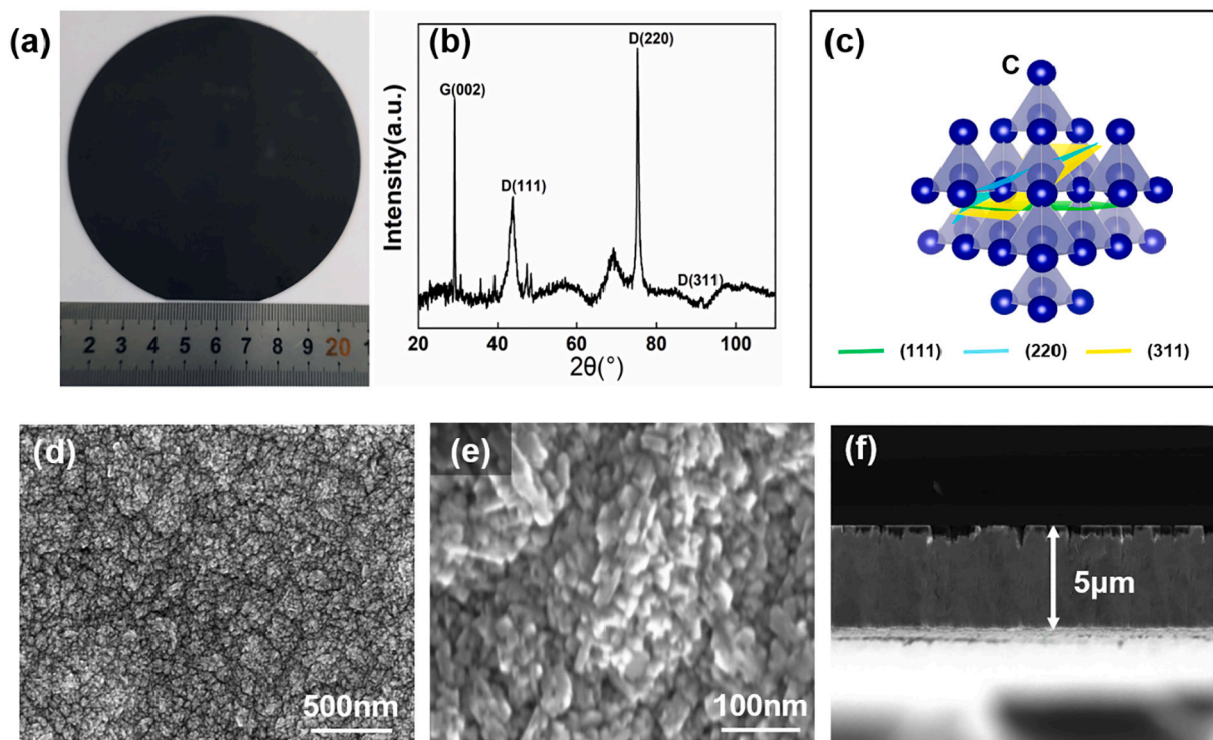


Fig. 2. (a) The macroscopic photograph of the diamond film on a 4-inch silicon substrate. (b) The XRD curve of the diamond film. (c) A schematic diagram of the crystal structure of the diamond film. (d and e) SEM images of the synthesized diamond film. (f) The cross-sectional view of the diamond film with the thickness of 5 μ m.

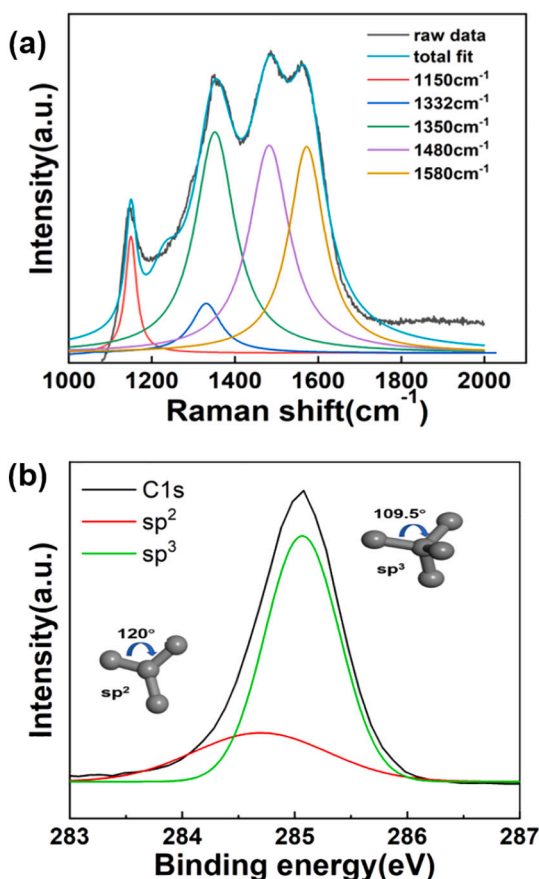


Fig. 3. (a) The Raman spectrum of the NCD films fitted by Lorentz multiple peaks at 1150 cm^{-1} , 1332 cm^{-1} , 1350 cm^{-1} , 1480 cm^{-1} and 1580 cm^{-1} . (b) The XPS C 1s spectrum is fitted with Gaussian function and is deconvoluted to two components with binding energy of 284.6 eV (for carbon sp^2 bonding) and 285.0 eV (for carbon sp^3 bonding).

photoelectron spectroscopy (XPS, ThermoFisher Scientific ESCALAB 250 \times) measurements were performed to characterize the surface structure and chemical composition of the NCD film. These analyzes were carried out at atmospheric pressure, with the Mg K α line ($h\nu = 1253.6\text{ eV}$) and with the analyzer pass energy set to 10 eV . Spectra fitting used Shirley's method to subtract the inelastic background of the C1s electron core-level. It also used no constraints with multiple Voigt profiles. Binding energies corrections used the hydrocarbon component of adventitious carbon fixed at 285.0 eV . The width at half maximum (FWHM) varied between 1.0 and 1.8 eV and the estimated accuracy of the peak positions was $\pm 0.1\text{ eV}$. The subtracted background was of "Shirley" type.

2.3. TERS measurement

It was performed on an AFM-based tip-enhanced Raman system (Horiba) as shown in Fig. 1. The excitation light at 532 nm was focused on the tip through an objective (Mitutoyo, M Plan Apo $100\times$, $\text{NA} = 0.7$) mounted at 45° . The TERS tip is a silver-covered silicon cone. The laser power at the focal volume was $\sim 1\text{ mW}$. The tip, controlled by the AFM cantilever, was operated in tapping mode to avoid damaging the sample. The scanning rate was set to 0.5 Hz to attenuate the shear force on the sample during scanning. An optical grating of 1800 g mm^{-1} was used for TERS measurements, and the integration time for spectrum acquisition was 1 s .

3. Results and discussion

Fig. 2a presents the macroscopic photograph of the as-grown diamond film on a 4-in. silicon substrate. The obtained X-ray diffraction pattern is presented in Fig. 2b. Three main peaks at $2\theta = 43.93^\circ$, 75.30° and 91.48° of the pattern are attributed to the diamond crystal structure D (111), D (220) and D (311) (the corresponding lattice planes are marked by the colors of green, blue and yellow, respectively, in Fig. 2c), while the peak at $2\theta = 26.55^\circ$ identified by the graphite structure G (200) illustrates the existence of a graphite phase in the diamond film [31]. The morphology and cross section of the diamond film was observed by scanning electron microscope (FEI Helios 600I). It can be seen from Figs. 2d and 1e that the diamond film clearly shows a uniform NCD structure with a grain size of less than $\sim 50\text{ nm}$. Fig. 2f is a cross-sectional view of the NCD film with a thickness of $5\text{ }\mu\text{m}$. It should be noted that the grain size of NCD in our experiments does not increase with the increase in film thickness, because the secondary nucleation rate of NCD is much greater than the growth rate of existing grains. This growth behavior is different from that of conventional microcrystalline diamond, in that the secondary nucleation rate is slow, and the grain size and roughness change rapidly with the increase of film thickness [32].

Fig. 3a presents a typical Raman spectrum from the NCD film, which is fitted by the Lorentzian function. It exhibits the typical characteristics of NCD structure with a weak sp^3 diamond Raman band $\sim 1332\text{ cm}^{-1}$ embedded with strong sp^2 graphite D and G bands at $\sim 1350\text{ cm}^{-1}$ and 1580 cm^{-1} , respectively. This result is consistent with previous results that the effects from the sp^2 -bonded carbon dominate all spectra, because the cross-section of the sp^2 phase is much higher than that of the sp^3 phase in visible Raman spectra [33–35]. Thus, even the spectra of diamond films mainly composed of sp^3 -bonded carbon show no direct evidence for the sp^3 configuration but are dominated by the sp^2 features. This assumption was also confirmed by our result of the XPS. Fig. 3b shows the XPS spectrum of C 1s which is deconvoluted by Gaussian multiple peaks fitting in a weak component with binding energy 284.6 eV (for carbon sp^2 bonding) and a strong one with binding energy 285.0 eV (for carbon sp^3 bonding) [36,37]. This result indicates that the main chemical composition of the NCD film in our experiments is a crystalline diamond structure. In addition, it should be noticed that there are two Raman bands at 1150 cm^{-1} and 1480 cm^{-1} defined as ν_3 and ν_1 , respectively, in Fig. 3b. Kuzmany et al. have provided clear evidence that ν_1 and ν_3 modes originate from *trans*-polyacetylene (TPA) in diamond films through the result of H–D isotope substitution [14]. And both ν_1 and ν_3 bands are characteristic of the motion of conjugate polymer skeletons with a substantial contribution from the stretching vibrations of the double carbon-carbon bonds.

Next, we present Raman analysis of the NCD film with a spatial resolution of nanoscale. The measurements were performed on an AFM-based tip-enhanced Raman system (Horiba) which is schematic in Fig. 1. The TERS tip is a silver-covered silicon cone with a radius of curvature about 100 nm (the inset of Fig. 1).

Fig. 4a shows the AFM surface morphology of the NCD film, which indicates that the NCD film is formed by the coalescence of circle diamond crystal clusters composed of smaller grains. The size of clusters is in the range of about $100\text{--}260\text{ nm}$. For TERS measurements, we chose the sample area within the red square shown in Fig. 4a, where are two diamond clusters. Fig. 4b and c show a magnified AFM image and a corresponding TERS image constructed with the Raman intensity area. As seen in the figures, completely different patterns are observed for both images in terms of their nanoscale characteristics. We observed a higher TERS signal intensity in the area around the two clusters (red dash circles) compared to that inside clusters in Fig. 4c. Fig. 4d shows a set of TERS spectra across the range between two clusters (positions are marked by red dots in Fig. 4b). Through comparing these Raman spectra, it can be found that all resonant Raman modes from the area between two clusters (positions 2 and 3) systematically became stronger. In addition, the ν_3 band at 1150 cm^{-1} inside the clusters (positions 1

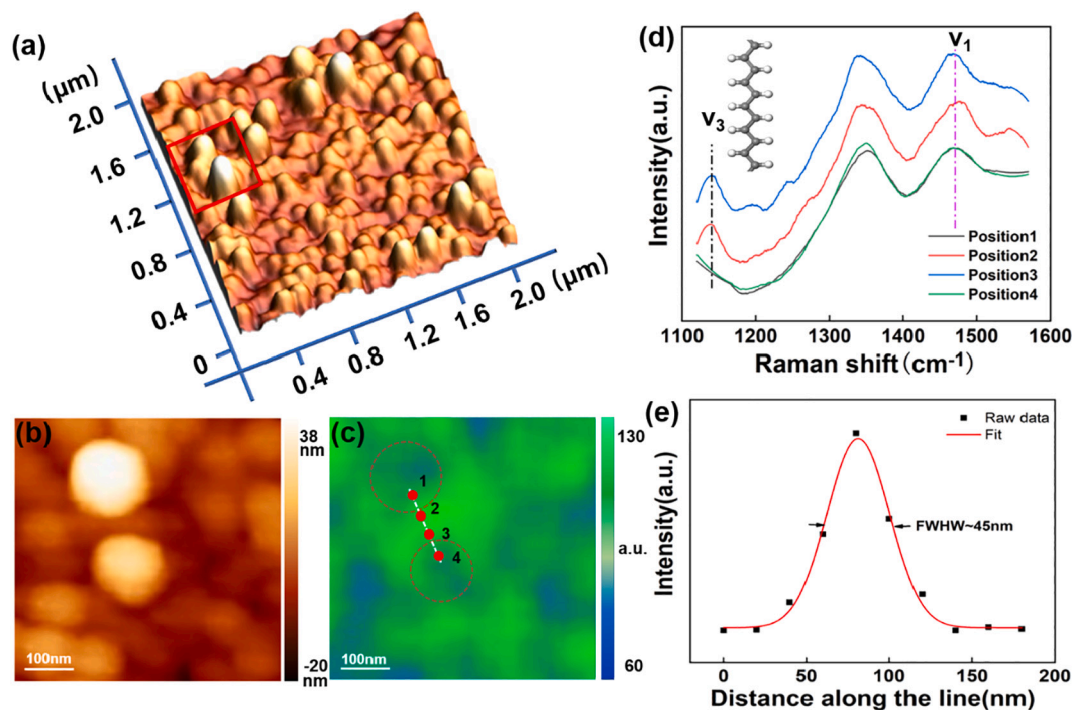


Fig. 4. AFM and TERS images of the diamond film. (a) The AFM image of the NCD film. (b) The magnified AFM image of the local area marked by the red square in (a). (c) The corresponding TERS image of (b). (d) TERS spectra from different position as marked by number in (c). (e) The TERS signal profile along the white line in (c).

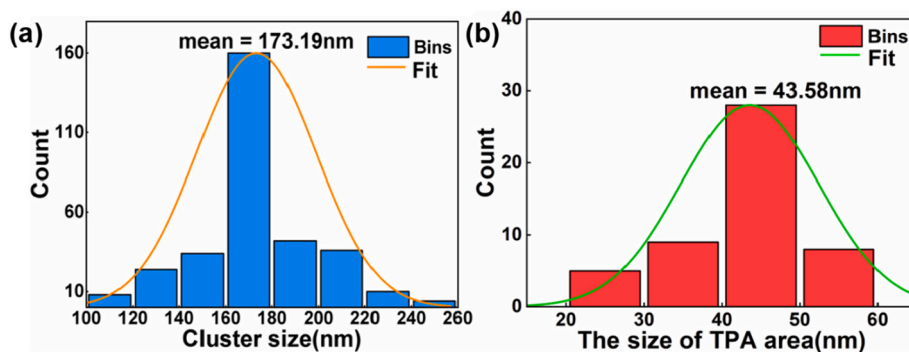


Fig. 5. (a) The size distribution histogram of clusters in the diamond film. (b) The size distribution histogram of TPA area.

and 4) is disappeared and the ν_3 band at 1480 cm^{-1} shows a tiny change. The similar experimental result has been observed in the earlier study for demonstrating the formation of TPA components at grain boundaries and the surface of NCD films. So this result implies that the increase in the TERS signal intensity mainly result from the contribution of TPA component on the surface of the NCD film. And ν_1 and ν_3 modes can be used as a fingerprint identification of the locally spatial distribution of TPA segments in nanoscale. In addition, according to the line profile of the white dashed line in Fig. 4e, we measured the area of TPA segments to be about 45 nm wide. Fig. 5a and b are the size distribution histograms of clusters and TPA areas in the NCD film, which were obtained by analyzing the AFM and TERS signals, respectively, from Fifty different ranges on the surface. The histograms show the size peaks of about 173 nm and 44 nm for clusters and TPA areas, respectively.

At last, it is worth to talk more about the possible role of TPA in the diamond synthesis reaction. In fact, our observation of the disappearance of ν_3 vibration band of TPA in the diamond clusters is very similar to the Raman spectra of microcrystalline diamond films composed of micro-sized grains [38]. According to Frenklach's mechanism and the

selection rule of vibrations [39,40], Sun et al. have proposed that the grown diamond (111) facet consists of (111) faces and {110} face steps, and the out-plane C—H stretch vibration characterizes the kernel formation while the in-plane C—H bending vibration does the propagation stages. So the disappearance of ν_3 vibration band of TPA in our measurements may be attributed to that the kernel formation along (111) faces is dominant over propagation growth along {110} face steps inside diamond clusters, due to the small grain size or a high secondary nucleation rate. On the other hand, because the chemical bond in TPA strongly differs from the bond in usual covalent carbon species, there would be a difference between the reactivity of TPA when opposed to diamond surfaces and usual carbon containing compounds. In that sense, the additional theoretical and experimental efforts, therefore, will need to be carried out in order to understand the role of TPA in the diamond synthesis reaction in nanoscale.

Many previous experiments were aimed to understand the Raman spectra of TPA of classically synthesized carbon materials. For example, it has been demonstrated that the deposited TPA is composed of chains exhibiting short conjugation lengths by using surface enhanced Raman

spectroscopy (SERS) [41]. With the help of TERS, however, one can obtain the spatial distribution of TPA segments with a high resolution in nanoscale. While the spatial resolution of TERS in our experiments is about 20 nm, it could not be the limit of this technique. With functionalized or sharper tips, it is able to become better, which will allow for more accurately characterizing the surface of NCD films in nanoscale.

4. Conclusions

In summary, we performed resonant TERS imaging of NCD films grown by HFCVD with a high spatial resolution. It was found that the NCD films in our experiments are consisted with crystalline clusters with a mean diameter of ~173 nm and TPA area with a mean width of ~44 nm. We demonstrated the advantage of TERS for nanoscale imaging of TPA segments of NCD films and identification of its chemical composition. Our work provides fundamental information for further studies of TPA segments to understand its role in the growth dynamics or physical properties of NCD films in future.

CRediT authorship contribution statement

Changzhi Gu: Conceptualization, Supervision.

Yang Guo: Writing - Review & Editing.

Junjie Li: Supervision.

Leiyong Hu: Writing - Original Draft, Data Curation, Visualization.

Shuo Du: Software, Validation, data Curation.

Shibing Tian: Data Curation.

Declaration of competing interest

The authors declare that they have no known competing financial interests or personal relationships that could have appeared to influence the work reported in this paper.

Acknowledgements

This work was supported by the National Key Research and Development Program of China under Grant Nos. 2016YFA0200400, 2016YFA0200800, the National Natural Science Foundation of China under Grant No. 61888102, 12074420 and 11674387; Strategic Priority Research Program of the Chinese Academy of Sciences under Grant No. XDB33000000 and Key Research Program of Frontier Sciences, CAS, Grant No. QYZDJ-SSWSLH042.

References

- [1] Y. Yue, Y. Gao, W. Hu, B. Xu, J. Wang, X. Zhang, Q. Zhang, Y. Wang, B. Ge, Z. Yang, Hierarchically structured diamond composite with exceptional toughness, *Nature* 582 (7812) (2020) 370–374.
- [2] J. Anaya, S. Rossi, M. Alomari, E. Kohn, L. Toth, B. Pecz, K.D. Hobart, T. J. Anderson, T.I. Feygelson, B.B. Pate, Control of the in-plane thermal conductivity of ultra-thin nanocrystalline diamond films through the grain and grain boundary properties, *Acta Mater.* 103 (2016) 141–152.
- [3] A. Banerjee, D. Bernoulli, H. Zhang, M.F. Yuen, J. Liu, J. Dong, F. Ding, J. Lu, M. Dao, W. Zhang, Ultralarge elastic deformation of nanoscale diamond, *Science* 360 (6386) (2018) 300–302.
- [4] K. Larsson, Y. Tian, Effect of surface termination on the reactivity of nano-sized diamond particle surfaces for bio applications, *Carbon* 134 (2018) 244–254.
- [5] Y. Wu, Y. Lin, A.A. Bol, K.A. Jenkins, F. Xia, D.B. Farmer, Y. Zhu, P. Avouris, High-frequency, scaled graphene transistors on diamond-like carbon, *Nature* 472 (7341) (2011) 74–78.
- [6] A. Karvounis, V. Nalla, K.F. MacDonald, N.I. Zheludev, Ultrafast coherent absorption in diamond metamaterials, *Adv. Mater.* 30 (14) (2018).
- [7] V.N. Mochalin, O. Shenderova, D. Ho, Y. Gogotsi, The properties and applications of nanodiamonds, *Nat. Nanotechnol.* 7 (1) (2012) 11–23.
- [8] A.C. Taylor, R. Edgington, R.B. Jackman, Patterning of nanodiamond tracks and nanocrystalline diamond films using a micropipette for additive direct-write processing, *ACS Appl. Mater. Interfaces* 7 (12) (2015) 6490–6495.
- [9] C. Chen, Y. Tzeng, E. Kohn, C. Wang, J. Mao, RF MEMS capacitive switch with leaky nanodiamond dielectric film, *Diam. Relat. Mater.* 20 (4) (2011) 546–550.
- [10] F. Cleri, Atomic and electronic structure of high-energy grain boundaries in silicon and carbon, *Comput. Mater. Sci.* 20 (3–4) (2001) 351–362.
- [11] M. Mohr, L. Daccache, S. Horvat, K. Brühne, T. Jacob, H.J. Fecht, Influence of grain boundaries on elasticity and thermal conductivity of nanocrystalline diamond films, *Acta Mater.* 122 (2017) 92–98.
- [12] S. Osswald, G. Yushin, V. Mochalin, S.O. Kucheyev, Y. Gogotsi, Control of sp²/sp³ carbon ratio and surface chemistry of nanodiamond powders by selective oxidation in air, *J. Am. Chem. Soc.* 128 (35) (2006) 11635–11642.
- [13] A. Ferrari, J. Robertson, Origin of the 1 1 5 0 cm⁻¹ Raman mode in nanocrystalline diamond, *Phys. Rev. B* 63 (12) (2001) 121405.
- [14] R. Pfeiffer, Kuzmany, Evidence for trans-polyacetylene in nanocrystalline diamond films from H–D isotropic substitution experiments, *Appl. Phys. Lett.* 82 (2003) 4149.
- [15] M. Veres, S. Tóth, M. Koós, Grain boundary fine structure of ultrananocrystalline diamond thin films measured by Raman scattering, *Appl. Phys. Lett.* 91 (3) (2007), 031913.
- [16] K. Ganesan, P. Ajikumar, S. Srivastava, P. Magudapathy, Structural, Raman and photoluminescence studies on nanocrystalline diamond films: effects of ammonia in feedstock, *Diam. Relat. Mater.* 106 (2020) 107872.
- [17] C.K. Chiang, C. Fincher Jr., Y.W. Park, A.J. Heeger, H. Shirakawa, E.J. Louis, S. C. Gau, A.G. MacDiarmid, Electrical conductivity in doped polyacetylene, *Phys. Rev. Lett.* 39 (17) (1977) 1098.
- [18] A.J. Heeger, Nobel lecture: semiconducting and metallic polymers: the fourth generation of polymeric materials, *Rev. Mod. Phys.* 73 (3) (2001) 681.
- [19] S. Liu, B. Cirera, Y. Sun, I. Hamada, M. Müller, A. Hammud, M. Wolf, T. Kumagai, Dramatic enhancement of tip-enhanced Raman scattering mediated by atomic point contact formation, *Nano Lett.* 20 (8) (2020) 5879–5884.
- [20] B. Yang, G. Chen, A. Ghafoor, Y. Zhang, Y. Zhang, Y. Zhang, Y. Luo, J. Yang, V. Sandoghdar, J. Aizpurua, Z. Dong, J.G. Hou, Sub-nanometre resolution in single-molecule photoluminescence imaging, *Nat. Photonics* 117 (11) (2017) 7583–7613.
- [21] A. Fali, T. Zhang, J.P. Terry, E. Kahn, K. Fujisawa, B. Kabijs, S. Koirala, Y. Ghafouri, D. Zhou, W. Song, L. Yang, M. Terrones, Y. Abate, Photodegradation protection in 2D in-plane heterostructures revealed by hyperspectral nanoscale imaging: the role of nanointerface 2D alloys, *ACS Nano* 15 (2) (2021) 2447–2457.
- [22] M. Richard-Lacroix, Y. Zhang, Z. Dong, V. Deckert, Mastering high resolution tip-enhanced Raman spectroscopy: towards a shift of perception, *Chem. Soc. Rev.* 46 (13) (2017) 3922–3944.
- [23] A. Bhattarai, A. Krayev, A. Temiryazev, D. Evplov, K.T. Crampton, W.P. Hess, P. Z. El-Khoury, Tip-enhanced Raman scattering from nanopatterned graphene and graphene oxide, *Nano Lett.* 18 (6) (2018) 4029–4033.
- [24] J. Stadler, T. Schmid, R. Zenobi, Nanoscale chemical imaging of single-layer graphene, *ACS Nano* 5 (10) (2011) 8442–8448.
- [25] S. Heeg, L. Shi, L.V. Poulikakos, T. Pichler, L. Novotny, Carbon nanotube chirality determines properties of encapsulated linear carbon chain, *Nano Lett.* 18 (9) (2018) 5426–5431.
- [26] M. Liao, S. Jiang, C. Hu, R. Zhang, Y. Kuang, J. Zhu, Y. Zhang, Z. Dong, Tip-enhanced Raman spectroscopic imaging of individual carbon nanotubes with subnanometer resolution, *Nano Lett.* 16 (7) (2016) 4040–4046.
- [27] A. Rosenkranz, L. Freeman, S. Fleischmann, F. Lasserre, Y. Fainman, F.E. Talke, Tip-enhanced Raman spectroscopy studies of nanodiamonds and carbon onions, *Carbon* 132 (2018) 495–502.
- [28] A. Rosenkranz, L. Freeman, B. Suen, Y. Fainman, F.E. Talke, Tip-enhanced Raman spectroscopy studies on amorphous carbon films and carbon overcoats in commercial hard disk drives, *Tribol. Lett.* 54 (2018) 66.
- [29] K. Zhang, Z. Xu, A. Rosenkranz, Y. Song, T. Xue, F. Fang, Surface- and tip-enhanced Raman scattering in tribology and lubricant detection—a prospective, *Lubricants* 7 (2019) 81.
- [30] T. Hao, W. Li, Z. Liu, Y. Sun, L. Jin, J. Li, C. Gu, Low turn-on field nanodiamond conical field emitter, *Diam. Relat. Mater.* 75 (2017) 91–95.
- [31] O.C. Wachesk, C.C. Wachesk, C.R. Hurtado, D.D. Damm, CVD-diamond nanoparticle synthesis for DLC film application, *J. Nanopart. Res.* 22 (2020) 293.
- [32] H. Zeng, P.U. Arumugam, S. Siddiqui, J.A. Carlisle, Low temperature boron doped diamond, *Appl. Phys. Lett.* 102 (22) (2013) 223108.
- [33] N. Wada, P. Gaczi, S. Solin, “Diamond-like” 3-fold coordinated amorphous carbon, *J. Non-Cryst. Solids* 35 (1980) 543–548.
- [34] A.C. Ferrari, J. Robertson, Interpretation of Raman spectra of disordered and amorphous carbon, *Phys. Rev. B* 61 (20) (2000) 14095.
- [35] J. Robertson, Diamond-like amorphous carbon, *J. Mater. Sci. Eng.* 37 (4–6) (2002) 129–281.
- [36] D. Barbosa, P. Hammer, V. Trava-Airoldi, E. Corat, The valuable role of renucleation rate in ultrananocrystalline diamond growth, *Diam. Relat. Mater.* 23 (2012) 112–119.
- [37] B. Humbert, N. Hellala, J.J. Ehrhardt, S. Barrat, E. Bauer-grosse, X-ray photoelectron and Raman studies of microwave plasma assisted chemical vapour deposition (PACVD) diamond films, *Appl. Surf. Sci.* 254 (20) (2008) 6400–6409.
- [38] P. Joshi, A. Haque, S. Gupta, R.J. Narayan, J. Narayan, Synthesis of multifunctional microdiamonds on stainless steel substrates by chemical vapor deposition, *Carbon* 171 (2021) 739–749.
- [39] M. Frenklach, K.E. Spear, Growth mechanism of vapor-deposited diamond, *J. Mater. Res.* 3 (1) (1988) 133–140.
- [40] B. Sun, X. Zhang, Z. Lin, Growth mechanism and the order of appearance of diamond (111) and (100) facets, *Phys. Rev. B* 47 (15) (1993) 9816.
- [41] T. Lopez-Rios, E. Sandre, S. Leclercq, E. Sauvain, Polyacetylene in diamond films evidenced by surface enhanced Raman scattering, *Phys. Rev. Lett.* 76 (26) (1996) 4935.